Improved cycling stability of ferrocene intercalated layered double hydroxides electrodes in aqueous electrolytes

Patrick Gerlach, Camille Douard, Elodie Grange, Laurence Athouël, Julien Sarmet, Philippe Stevens, Gwenaëlle Toussaint, Fabrice Leroux, Christine Tavoit-Gueho, Thierry Brousse

To cite this version:

Patrick Gerlach, Camille Douard, Elodie Grange, Laurence Athouël, Julien Sarmet, et al.. Improved cycling stability of ferrocene intercalated layered double hydroxides electrodes in aqueous electrolytes. Electrochimica Acta, 2025, 538, pp.146962. ⟨10.1016/j.electacta.2025.146962⟩. ⟨hal-05214445⟩

HAL Id: hal-05214445

https://hal.science/hal-05214445v1

Submitted on 19 Aug 2025

HAL is a multi-disciplinary open access archive for the deposit and dissemination of scientific research documents, whether they are published or not. The documents may come from teaching and research institutions in France or abroad, or from public or private research centers.

L'archive ouverte pluridisciplinaire **HAL**, est destinée au dépôt et à la diffusion de documents scientifiques de niveau recherche, publiés ou non, émanant des établissements d'enseignement et de recherche français ou étrangers, des laboratoires publics ou privés.

Distributed under a Creative Commons CC BY 4.0 - Attribution - International License

Improved Cycling Stability of Ferrocene Intercalated Layered Double Hydroxides Electrodes in Aqueous Electrolytes

Patrick Gerlach[1,2], Camille Douard[1,2], Elodie Grange[1], Laurence Athouël[1,2], Julien Sarmet[3], Philippe Stevens[2,4], Gwenaëlle Toussaint[2,4], Fabrice Leroux[3], Christine Tavoit-Gueho[3], Thierry Brousse[1,2]*

1 Nantes Université, CNRS, Institut des Matériaux de Nantes Jean Rouxel, IMN, 2 rue de la Houssinière BP32229, CEDEX 3, F-44322 Nantes, France

2 Réseau sur le Stockage Electrochimique de l'Energie (RS2E), CNRS FR 3459, 33 rue Saint Leu, CEDEX, F-80039 Amiens, France

3 Université Clermont Auvergne, Institut de Chimie de Clermont-Ferrand (ICCF) UMR n°6296, Clermont Auvergne INP, CNRS, Institut Pascal, F-63000 Clermont-Ferrand, France

4 EDF R&D, Department LME, Avenue des Renardières, CEDEX, F-77818 Moret-sur-Loing,

*corresponding author Thierry Brousse, thierry.brousse@univ-nantes.fr

Abstract

Through two redox molecules, mono- and dicarboxylic ferrocene anions (FcMono and FcDi, respectively), interleaved between the lamellae of a layered double hydroxide $Mg_2Al(OH)_6$ (LDH), have been synthesized and investigated as electrode materials inwater in salt electrolyte using lithium bis-(trifluoromethanesulfonyl)-imide $Li^+[N(SO_2CF_3)_2]^-$ (LiTFSI) mixed in different amount of H_2O. The redox activities of the composite electrode materials including $Mg_2Al(OH)_6[FcMono]_{1.0}$ and $Mg_2Al(OH)_6[FcDi]_{0.5}$ suffer from the dissolution of the active redox species migrating out of the host structure in water based electrolyte when low molalities are used. However, while increasing the molality of the electrolyte solution $Mg_2Al(OH)_6[FcDi]_{0.5}$ electrode material performs better than $Mg_2Al(OH)_6[FcMono]_{1.0}$ ones according to the cycling stability For $Mg_2Al(OH)_6[FcDi]_{0.5}$, an optimum behavior is observed for a concentration of LITFSI of at least of 10 m . The electrode exhibits a stable capacity of 25 mAh g^{-1} which is maintained after more than 100 cycles with 100 % coulombic efficiency. Such stability during cycling is explained by two complementary processes: the preservation of the lamellar structure of $Mg_2Al(OH)_6[FcDi]_{0.5}$, FcDi molecule being tethered by its two ends (unlike FcMono tethered at one end only), in connection with the high concentration of the electrolyte in LiTFSI, which helps slowing down the migration of the interleaved redox species out of the structure. This opens the route to re-evaluate LDH-based hybrid materials for water-based energy storage devices.

1. Introduction

Layered double hydroxides (LDHs) are brucite type ($Mg(OH)_2$) layered materials, which follow the general formula $[M^{2+}_{1-x}M^{3+}_x(OH)_2]^{z+}(A^{n-})_{z/n} \cdot y\ H_2O$, where M^{2+} and M^{3+} are divalent and trivalent metals cations. Since the $[M^{2+}_{1-x}M^{3+}_x(OH)_2]^{z+}$ layers bear a net positive charge, A^{n-} anions are intercalated between the metal hydroxide layers to ensure charge compensation of the material [1–9]. A common example of this structure is hydrotalcite $[Mg_6Al_2(OH)_{16}]CO_3 \cdot 4\ H_2O$ (x = 0.25) [10].

LDHs have been investigated for many applications such as ion exchange [11–13] , drug delivery [14–17], water purification [18–22], polymer [23–25] or anti corrosion [26–29] additives, sensors [30–35] and catalysis [36–50]. The same is true for LSH in energy storage application [51,52] in batteries [53–63] and high power hybrid devices [64–74].

The pioneering work by Mousty et al.,where organic redox active moieties were inserted into LDHs structures led to the production of a new type of sensor [75]. Inspired by this work, we presented the two model LDH materials $Mg_2Al(OH)_6[FcMono]_{1.0}$ x 3.6 H_2O and $Mg_2Al(OH)_6[FcDi]_{0.5}$ x 2 H_2O, which will be referred to MgAl-FcMono and MgAl-FcDi [76–80]. The structure of both MgAl-FcMono and MgAl-FcDi was recently reported [79].

These two LDH's utilize the redox activity of the inserted ferrocene group for energy storage [81–88]. Even though the intercalation of redox active ferrocene anions during synthesis was successful and their electrochemical activity in the $MgAl(OH)_6$ structure for electrodes based on MgAl-FcMono and MgAl-FcDi has been demonstrated, stable charge/ discharge cycles were not observed [78]. The first cycle has a capacity close to the theoretical values of 56.7 and 37.5 mAh g^{-1} for MgAl-FcMono and MgAl-FcDi respectively, thus indicating that the lamellar confinement does not impede the redox activity of the interleaved species. However, this capacity drops significantly right from the first discharge and subsequent cycles [79]. This loss in specific capacity during cycling is caused by the dissolution of the ferrocene compound into the aqueous electrolyte as explained in our previous studies [77,79].

In a recent work, we found that highly concentrated electrolytes like ionic liquids can hinder this dissolution and therewith increase the cycling stability for both MgAl-FcMono and MgAl-FcDi based electrodes [79]

In this work, we scrutinize the behavior of MgAl-FcMono and MgAl-FcDi based electrodes in dilute electrolytes like 1M LiTFSI in H_2O and highly concentrated ones like neat ionic liquids. In doing so, we aim to highlight the positive effects of the higher concentrated electrolytes on the cycling stability of MgAl-FcMono and MgAl-FcDi. For this purpose, we tested MgAl-FcMono and MgAl-FcDi based electrodes in the five electrolytes 1, 5, 10, 15, 21 molal LiTFSI in H_2O (mol of salt per kg of solvent). This should help to define the best compromise between capacity, power capability and cycling ability of the electrodes since based on our previous results [79], highly concentrated water-in-salt electrolytes should provide a higher stability.

2. Experimental

MgAl-FcMono and Di were prepared using a coprecipitation method as reported elswhere.[79] The synthesis reactor was pre-filled with 100 mL of ferrocene solution (0.02 mol L^{-1} FcMono or 0.01 mol L^{-1} FcDi) in water and the pH was initially adjusted to 9.5 using 1 mol L^{-1} NaOH solution. The cation solution prepared from chloride salts (0.333 mol L^{-1} $MgCl_{2,}6H_2O$ and 0.167 mol L^{-1} in $AlCl_3$, $_,6H_2O$) was added drop-wise (0,05 mL min^{-1}) to the reactor at 25 °C using peristaltic pumps, under magnetic stirring and a nitrogen atmosphere. 10 mL of this solution were added so that $n_{Fc} = 4n_{Al}$ in the final solution. The pH of the reaction mixture was kept constant at 9.5 by the simultaneous addition of 1 mol L^{-1} NaOH solution. An ageing time of 24 hours was applied, whilst the solution was stirred, after which the precipitate was recovered by three washing/centrifugation cycles and then dried in oven at 40°C in air.

The working electrodes were prepared with a composition of 60 wt% LDH, 30 wt% carbon black and 10 wt% binder. To do so, MgAl-FcMono or MgAl-FcDi were mixed with conductive additive (Super Graphite, Superior Graphite Co.) in 20 ml Ethanol (EtOH) to form a suspension, which was rotated horizontally overnight in a closed glass vial with glass beads (d =2 mm) to ensure homogenization between the two components. The suspension was then dried in an oven at 60 °C for 3 h. PTFE (Sigma Aldrich) was added to the dried residue in the form of a 60 % suspension in water to form the composite electrodes. This mixture was mixed in a mortar with the addition of a few drops of EtOH for 10 min. The resulting dough was kneaded, rolled out and folded several times on a glass plate to create a mechanically stable sheet. After the final roll out, electrodes with a diameter of 8 mm were punched out. After drying at 60°C overnight, these electrodes resulted in a final area of 0.5 cm^2, a thickness of 200 µm and an average mass loading of 12 mg cm^{-2}.

The counter electrodes used in the cells were oversized self-standing carbon electrodes. For their preparation, activated carbon (YP50, Kuaray), carbon black (Super Graphite, Superior

Graphite Co.) and PTFE (Sigma Aldrich, 60% solution) were mixed in a weight ratio of 85:10:5 and 60 ml of EtOH were added to the mixture. The suspension so obtained was stirred at 70 °C until a dough was formed. This dough was transferred to a glass plate, kneaded, and folded as described above for the working electrode preparation. After the final roll out, electrodes with a diameter of 12 mm (1.13 cm^2) and a thickness of 1.3 mm were punched out. These electrodes had an average mass loading of 53 mg cm^{-2}.

The investigated electrochemical cells were assembled in a 3-electrode Swagelok setup. The working electrode was a LDH composite electrode, the counter electrode was the self-standing carbon electrode and a silver wire was used as the pseudo-reference electrode. A glass fiber separator (Whatman) filled with 150 µl of electrolyte separated the two electrodes.

Electrolytes were prepared by dissolving LiTFSI (Solvionic) in H_2O to produce 1, 5, 10, 15 and 21 molal solutions.

The viscosity was measured using a rheometer (Anton Paar, MCR 72) with a shear rate of 1000 1/s,

The ionic conductivities were measured by electrochemical impedance spectroscopy (EIS) using Biologic-VMP3 equipment with Swagelok cells and stainless steel blocking electrodes. A Teflon ring placed in the Swagelok cell allowed for the control of the form factor (3 mm x 110 mm2). The frequency ranged from 1 MHz to 100 mHz with a polarization amplitude of 20 mV. The measurements were performed at +23 °C in a thermally regulated room. The ionic conductivity σ (S.cm-1) was calculated from the resistance values obtained with the EIS, following the equation (1).

$$\sigma = t/(R\ S) \qquad (1)$$

Where t is the thickness of the electrolyte (cm), S the surface (cm^2) and R the resistance (Ω). An aqueous 1M KCl electrolyte was used as a standard with an ionic conductivity of 111 mS cm^{-1} at 23°C.

Electrochemical tests were performed using a multichannel potentiostatic-galvanostatic workstation (BioLogic Science Instruments, VMP3 with ECLab software) at room temperature. Before all electrochemical experiments, the cells were set to equilibrium by resting at open circuit (OCP) for 1 h.

Cyclic voltammetry (CV) experiments were performed at a scan rate of 1 mV s^{-1} in a voltage window of – 0.5 to 0.8 V vs. Ag. A ferrocene-free electrode prepared with the same composition has been tested in 1m LiTFSI aqueous electrolyte and the contribution is less than 1 C g^{-1} (0.3 mAh g^{-1}), mainly coming from carbon black additive. This value was not subtracted from the capacity values reported in the manuscript.

Constant current galvanostatic charge/discharge experiments were performed with a 1C rate, which is defined as the current needed to charge or discharge the electrode in 1 h with respect to the full utilization of the theoretical capacity of the LDH active materials (56.7 mAh g^{-1} for MgAl-FcMono and 37.5 mAh g^{-1} for MgAl-FcDi). For the calculation of the theoretical capacity of the electrode, the molar mass of the ideal structures of $Mg_2Al(OH)_6[FcMono]_{1.0}$ x 2 H_2O and $Mg_2Al(OH)_6[FcDi]_{0.5}$ x 2 H_2O have been used. Cycling has been carried out between -0.5 and 0.8 V *vs.* Ag.

3. Results and Discussion

At first, in order to understand the influence of the different concentrations of electrolytes on the electrochemical performance of the tested MgAl-FcMono and MgAl-FcDi based electrodes, the viscosity and ionic conductivity of 1m, 5m, 10m, 15m, 21m LiTFSI in H_2O were measured and depicted in Figure 2.

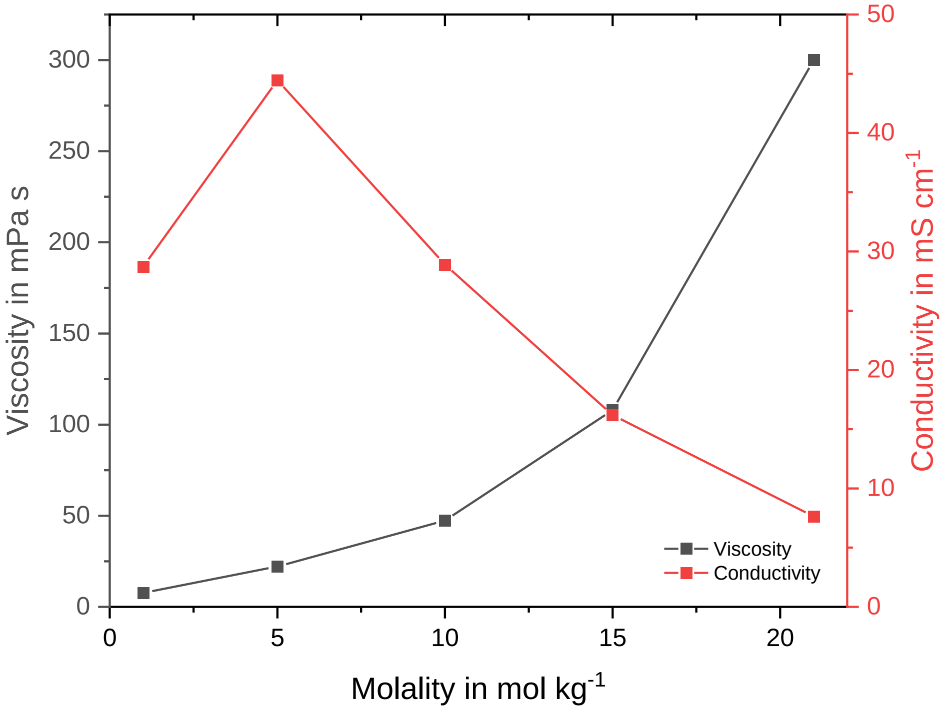

Figure 1 : Viscosity and conductivity of LiTFSI in H_2O electrolyte for molalities 1, 5, 10, 15 and 21m at 23°C in mol/kg of H_2O.

As expected, the viscosities of these aqueous electrolytes increase with increasing salt concentration. Thus, for a molality of 1m, 7.7 mPa s^{-1} were measured at a temperature of 23°C, whilst the maximum viscosity of 300 mPa s^{-1} is reached with the water-in-salt composition at 21m. The correlation of concentration and ionic conductivity on the contrary is not an increasing monotone. A maximum conductivity of 44.5 mS cm^{-1} is obtained at 5m. This value is similar to already reported ionic conductivity[89][90,91] (maximum value of 50 mS cm^{-1} for 5 molal LiTFSI in water), while Suo et al [92] reported a maximum ionic conductivity of 45 mS cm^{-1} for the same molality. The maximum ionic conductivity value was also measured for a lower molality (58 mS cm^{-1} at 4 molal)[93].

At higher molalities, the ionic conductivity decreases, which means that although a higher number of charge carriers is present, the dissolved ions are hindering each other. At 21m, a conductivity of 7.6 mS cm^{-1} is measured. From these results, the best electrochemical performance of MgAl-FcMono and MgAl-FcDi based electrodes should be obtained when 5m LiTFSI in H_2O is used as the electrolyte.

To verify this assumption, Figure 2 compares the electrochemical performances of the first and 50th CV cycle of MgAl-FcMono and MgAl-FcDi based electrodes using a scan rate of 1 mV s^{-1} in LiTFSI based aqueous electrolytes using molalities ranging from 1m to 21m.

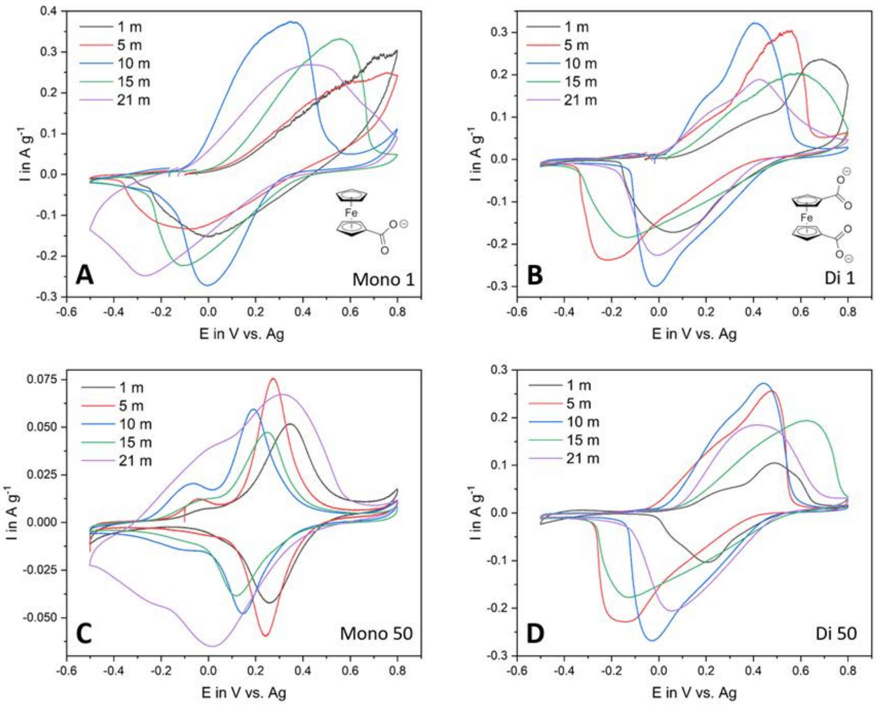

Figure 2: A and B) 1st, C and D) 50th CV cycle for MgAl-FcMono and MgAl-FcDi based electrodes in 1m, 5m, 10m, 15m and 21m LiTFSI in H_2O at 1 mV s^{-1}.

Figure 2A and B display the first cycle of MgAl-FcMono and MgAl-FcDi based electrodes in all tested electrolytes. For both materials, major differences in redox signals are visible with respect to the electrolyte concentration.

Figure 2A displays the highest current densities of all CV's presented in Figure 2, from which the peak specific currents can be measured. Using 10m LiTFSI in H_2O for example, leads to 0.37 A g^{-1} for the oxidation of ferrocene. However, during the corresponding reduction, only - 0.27 A g^{-1} was obtained. This phenomenon of much lower currents during the reduction process is present for all concentrations and indicates an irreversible reaction with low coulombic efficiencies in the first cycle.

Figure 2C shows the electrochemical behavior of MgAl-FcMono based electrodes after 50 CV cycles at 1 mV s^{-1}. The specific peak currents obtained range between -0.065 and 0.075 A g^{-1}

and reveal a significant loss in current, and thus redox activity, for all electrolyte concentrations.

In Figure 2B, similar peak currents as in Figure 2A are obtained for MgAl-FcDi. With 0.32 and -0.30 A g^{-1}, the highest currents are again measured in 10m LiTFSI in H_2O. However, in contrast to the results for MgAl-FcMono, reduction peaks for MgAl-FcDi show similar peak currents as the oxidation process. This indicates an improved reversibility of the redox reaction of ferrocene. In addition, this higher reversibility is retained in Figure 2D, where after 50 CV cycles, a much lower fade in peak intensity is shown. An exception from this are the redox peaks of MgAl-FcDi in 1 m LiTFSI in H_2O where the current is reduced to 0.1 and -0.1 A g^{-1}.

In general, it can be observed from these results that a higher cycling coulombic efficiency and cycling stability can be expected with MgAl-FcDi and with aqueous LiTFSI electrolyte concentrations higher than 1m compared to MgAl-FcMono or to low concentrations of LITFSI in the electrolyte.

The cyclic voltammetry experiments provide a first general indication of the electrochemical behavior of the MgAl-FcMono and MgAl-FcDi electrodes. Since the detailed discussion of every measured peak current, redox potential and peak shape of the resulting CVs would be complex and cluttered, Figure 3 summarizes this data and presents the calculated capacities of all plotted redox peaks with respect to the electrolyte concentrations.

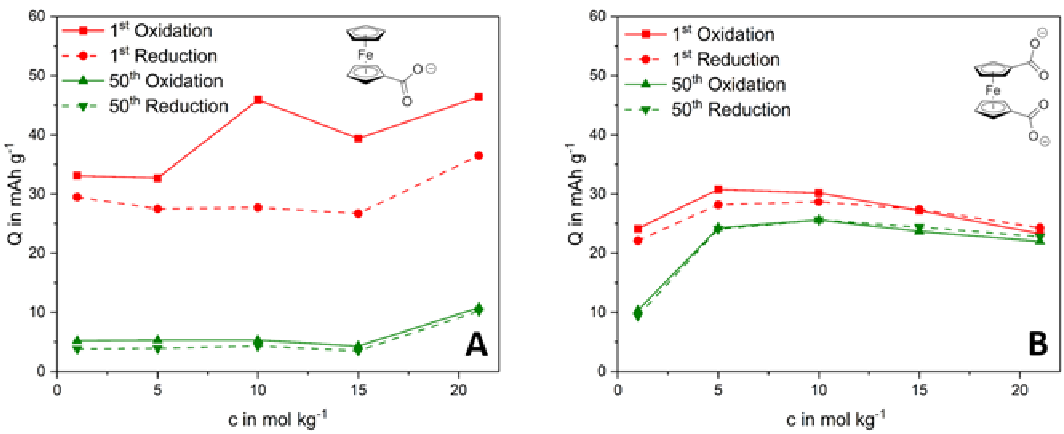

Figure 3 : Capacities calculated from CV's in Figure 3 for A) MgAl-FcMono electrode and B) MgAl-FcDi.

In general, higher capacities are obtained for the oxidation than for the corresponding reduction. Indeed, the oxidation of ferrocene into ferricenium species could lead to the release of these species in the electrolyte, which in turn will decrease the overall capacity of the electrode.

Figure 3A shows the first oxidation capacity and corresponding reduction of MgAl-FcMono in red, whilst the capacities after 50 cycles of CV at 1 mV s^{-1} are displayed in green. For the first CV cycle, an increase in oxidation capacity is observed when the electrolyte concentration is increased. The highest capacities are reported for 10 and 21 m. This result is surprising, since the highest ionic conductivity was measured for 5 m. In particular, the high initial capacity obtained at 21 m is contradictory to the low conductivity of 7.6 mS cm^{-1} at this concentration. For the first reductions, a loss in charge to a value of 28 mAh g^{-1} is recorded. Again, an exception is seen for 21 m, where 37 mAh g^{-1} are displayed upon reduction. Nevertheless, for all concentrations, a strong difference between oxidation and reduction capacities is calculated, indicative of low coulombic efficiencies for all CV's. It can be noted that the theoretical capacity of 56.7 mAh g^{-1} was never observed for MgAl-FcMono, and a maximum of 82% of this value was measured in 21 m electrolyte solution.

Much higher efficiencies are shown after 50 CV cycles but at much lower capacities. For the oxidations, however, only 5 mAh g^{-1} are obtained at 1 to 15m with corresponding 4 mAh g^{-1} on reduction revealing the low cycling stability of MgAl-FcMono. At 21m again, higher values of 11 and 10 mAh g^{-1} are obtained showing a lower decrease in capacity at higher molalities.

Figure 3B highlights the different behavior of MgAl-FcDi based electrodes. For the first CV, lower specific capacities are obtained, which is in line with the lower theoretical capacity of MgAl-FcDi. The highest capacities of 31 mAh g^{-1} are obtained during the oxidation in 5 and 10m LiTFSI in H_2O. Furthermore, the values of oxidation and reduction capacities are much closer yielding a higher coulombic efficiency than for MgAl-FcMono whatever the electrolyte concentration. The smallest capacity is measured in 1 and 21m electrolytes. The most evident difference in CV cycling between MgAl-FcMono and MgAl-FcDi is the much higher cycling stability of MgAl-FcDi over 50 CV cycles. Here an average 24 mAh g^{-1} is obtained with high efficiencies close to 100 % for 5 to 21m LiTFSI in H_2O. An exception is shown for the 1m electrolyte in which a much lower capacity of 9.9 mAh g^{-1} is measured. This reveals a reduced cycling stability of MgAl-FcDi in 1m LiTFSI in H_2O, while the cycling stability is drastically improved in more concentrated electrolyte. As for MgAl-FcMono, the theoretical capacity of 37.5 mAh g^{-1} for MgAl-FcDi was never achieved. A maximum of 82% of this value was measured in 5 m electrolyte, which is similar to what was measured for MgAl-FcMono in 21 m.

The findings of the CV experiments shown in Figure 2 and Figure 3 are verified in Figure 4 where the constant current galvanostatic charge discharge (CCGCD) plots of the first, second and 10^{th} charge/ discharge cycles at 1C of MgAl-FcMono and MgAl-FcDi are shown.

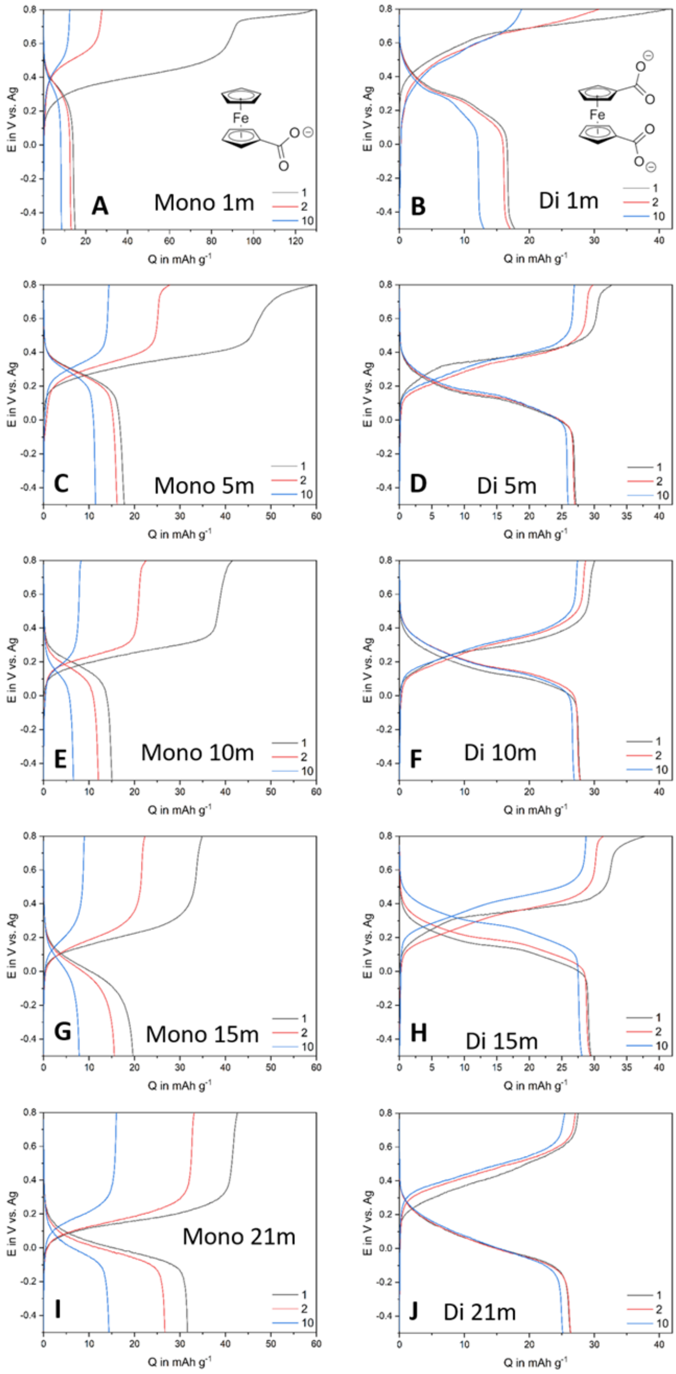

Figure 4 : Constant current galvanostatic charge discharge (CCGCD) profiles of charge/ discharge cycles 1, 2 and 10 for MgAl-FcMono and MgAl-FcDi based electrodes in A and B) 1m, C and D) 5m, E and F) 10m, G and H) 15m and I and J) 21m LiTFSI in H_2O at 1C.

Figure 4A displays the CCGCD profiles of MgAl-FcMono in 1m LiTFSI in H_2O. For the first charge a very high capacity of 128 mAh g^{-1} is presented, which is more than the double of the theoretical capacity of 56.7 mAh g^{-1}. At this lower LITFSI concentration, but higher H_2O concentration, a second oxidation plateau is observed which could correspond to an oxygen evolution reaction. Indeed, he usual potential vs Ag quasi reference electrode is close to +0.25 V vs NHE. At pH = 7, oxygen evolution reaction is supposed to occur at +0.81 V vs NHE, i.e. at +0.56 V vs the Ag quasi reference electrode. The observed plateau is located at a higher value as observed in Fig. 4A, B and C, which can be related to some overpotential for oxygen evolution reaction. Moreover, in the case of Fig. 4A, B and C, the oxidation took more than one hour which is 3 times longer than for the CV experiments. Thus, the electrodes are staying a longer time in a critical oxidation potential zone during the galvanostatic experiments compared to the CV experiments.

For the following reduction, however, only 15 mAh g^{-1} could be discharged (η = 12 %). On the second cycle, this capacity loss is not regained and continues. After 10 cycles only 13 mAh g^{-1} are stored during the charging process. This trend of capacity fade while cycling is reproduced for 5m, 10m, 15m and 21m (Figure 4C, E, G and I). However, with increasing LITFSI concentration (and lower H_2O concentration), this process is slowed down, with the highest capacity measured for MgAl-FcMono in 21m LiTFSI in H_2O after 10 cycles (43 and 32 mAh g^{-1}). As an indication, a molality of 21m has a molecular ratio of 1 LITFSI to only 2.6 H_2O whereas 1m has a H_2O:LITFSI ratio of 56.

MgAl-FcDi in 1m LITFSI (Figure 4B) mimics the behavior of MgAl-FcMono under the same conditions, but the second oxidation plateau is not clearly seen in this case. For the first charge, the theoretical capacity of 37.5 mAh g^{-1} is reached. Nevertheless, as seen in the previous graphs, the first reduction and subsequent cycles show a fast decline in capacity down to 18 mAh g^{-1}. On the contrary, beginning from 5m in Figure 4D, a lower initial charge capacity is measured but a much more stable cycling is displayed for MgAl-FcDi in higher concentrated electrolytes. For 5m, 10m, 15m and 21m LiTFSI in H_2O (Figure 4D, F, H and J), cycle 10 presents similar discharge capacities as during the first cycles.

Figure 5 displays the 100 subsequent charge/discharge cycles after the 10 first cycles previously shown in Figure 4 at 1 C for MgAl-FcMono and MgAl-FcDi for each concentration.

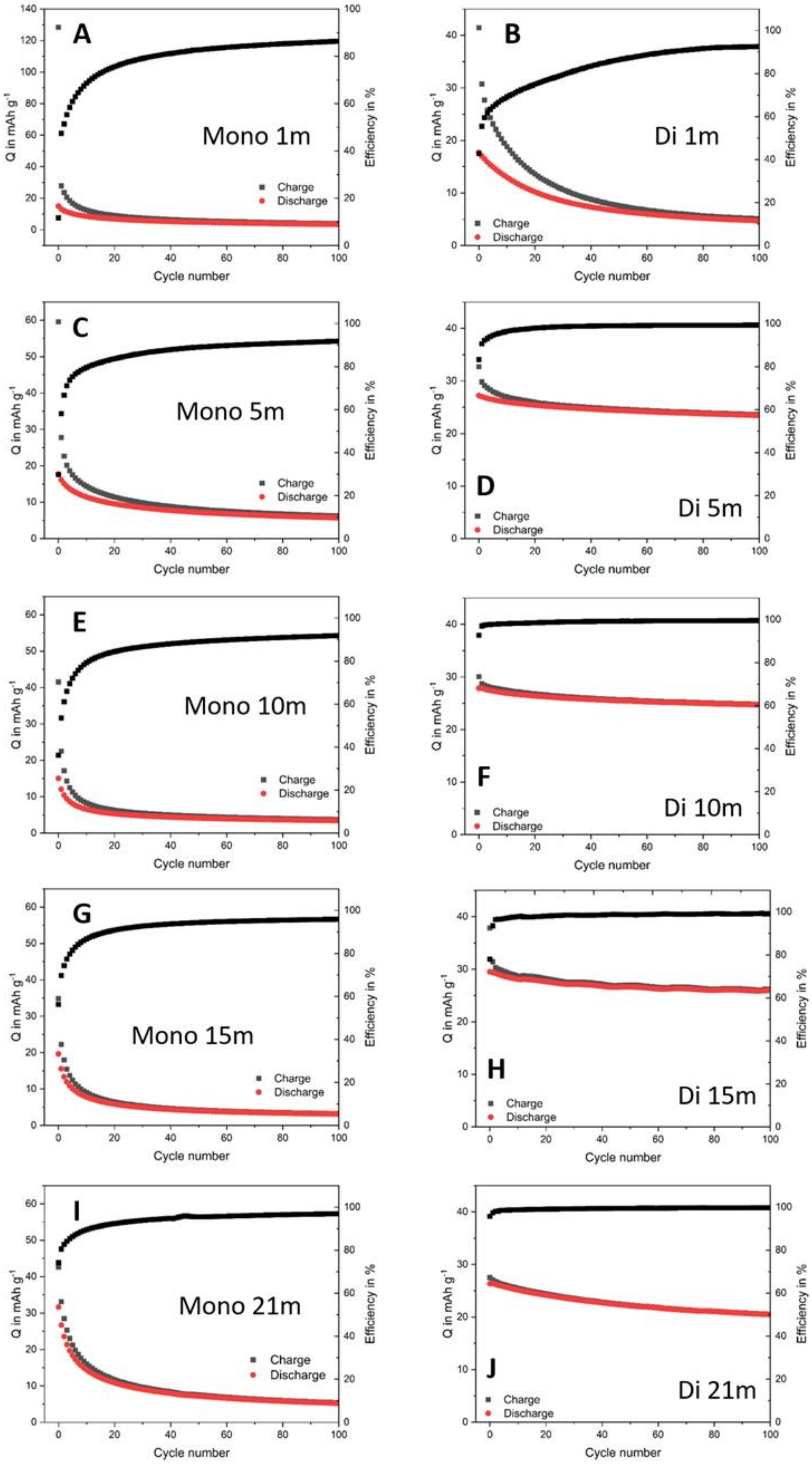
A
Mono 1m
B
Di 1m
C
Mono 5m
D
Di 5m
E
Mono 10m
F
Di 10m
G
Mono 15m
H
Di 15m
I
Mono 21m
J
Di 21m
Charge
Discharge
Q in mAh g-1
Efficiency in %
Cycle number

Figure 5 : Charge/ discharge cycling stability of MgAl-FcMono and MgAl-FcDi based electrodes in A and B) 1m, C and D) 5m, E and F) 10m, G and H) 15m and I and J) 21m LiTFSI in H_2O at 1C for 100 cycles.

In Figure 5 the tendencies shown in Figure 4 still remain. MgAl-FcMono based electrodes show a weakcycling stability over the course of 100 cycles at 1C. The highest stability is obtained with a 21m concentration. Furthermore, in all the MgAl-FcMono plots, a low coulombic efficiency is obtained upon the first 30 cycles whatever the concentration (Figures 5A, 5C, 5E, 5G, 5I).

Figure 5B displays a similar behavior in 1m LiTFSI in H_2O for MgAl-FcDi as the one observed for MgAl-FcMono. However, in 5m and higher concentrations (Figures 5D, 5F, 5H, 5J), a much more stable cycling with a higher coulombic efficiency are achieved upon 100 cycles. Therefore, stable cycling is possible using MgAl-FcDi in highly concentrated LITFSI electrolytes (> 1 m).

From these findings, it is clear that the cycling stability is influenced by the electrolyte concentration. Moreover, it seems that the MgAl-FcDi is able to sustain stable cycling at electrolyte concentration equal and higher than 5m unlike MgAl-FcMono which is still loosing capacity even at highly concentrated electrolyte. One possible explanation could be the stronger interaction of ferrocene di-carboxylate anions with the positively charged cationic layers: two negative charges on the anion enabling coulombic interactions with the upper cationic layer and the lower cationic layer. Mono-charged mono-carboxylate anions only interacts with one cationic layer, thus leading to a weaker interaction of the anions with the host structure. Ongoing in-situ measurements should provide further insights in the future in order to shed light on this phenomenon.

4. Conclusion

In this work, two LDH-based electrodes intercalated with redox active anions, $Mg_2Al(OH)_6[FcMono]_{1.0}$ and $Mg_2Al(OH)_6[FcDi]_{0.5}$ (MgAl-FcMono and MgAl-FcDi, respectively), were investigated in water-based electrolytes, namely 1, 5, 10, 15, 21 molal LiTFSI in H_2O. The redox activities of the composite electrode materials, suffer from the dissolution of the active redox species migrating out of the host structure when low molality electrolyted are used (< 5 m). However, while increasing the molality of the electrolyte solution, MgAl-FcDi electrode material exhibits a better stability upon cycling compared to MgAl-FcMono. An optimum behavior is observed for a concentration of LITFSI of at least of 10 m for MgAl-FcDi electrode with a stable capacity of 25 mAh g^{-1} over 100 cycles with 100 % coulombic efficiency. The strongest interaction of ferrocene di-carboxylate anion inside the LDH structure is suspected/likely to be responsible of such improved cycling stability. Such finding opens the way for re-evaluating LDH-based hybrid materials for water-based energy storage devices.

Acknowledgements

This research was funded by the French Research Agency ANR AAPG2020 “LaDHy”, ANR-20-CE05-0024-01. Labex STORE-EX (ANR-10-LABX-76-01) is also acknowledged for financial support. Conseil Régional des Pays de la Loire is also acknowledged for financial support within the framework of "trajectoires nationales" project funding.

References

[1] Z. Gu, J. J. Atherton, Z. P. Xu, *Chem. Commun.* **2015**, *51*, 3024–3036.
[2] A. I. Khan, D. O’Hare, *J. Mater. Chem.* **2002**, *12*, 3191–3198.
[3] X. Guo, F. Zhang, D. G. Evans, X. Duan, *Chem. Commun.* **2010**, *46*, 5197.
[4] S. J. Mills, A. G. Christy, J.-M. R. Génin, T. Kameda, F. Colombo, *Mineral. mag.* **2012**, *76*, 1289–1336.
[5] Q. Wang, D. O’Hare, *Chem. Rev.* **2012**, *112*, 4124–4155.
[6] A. I. Khan, A. Ragavan, B. Fong, C. Markland, M. O’Brien, T. G. Dunbar, G. R. Williams, D. O’Hare, *Ind. Eng. Chem. Res.* **2009**, *48*, 10196–10205.
[7] M. Duan, S. Liu, Q. Jiang, X. Guo, J. Zhang, S. Xiong, *Chinese Chemical Letters* **2022**, *33*, 4428–4436.
[8] C. Taviot- Guého, V. Prévot, C. Forano, G. Renaudin, C. Mousty, F. Leroux, *Adv Funct Materials* **2018**, *28*, 1703868.
[9] G. R. Williams, D. O’Hare, *J. Mater. Chem.* **2006**, *16*, 3065.
[10] F. Cavani, F. Trifirb, A. Vaccari, **n.d.**
[11] A. V. Radha, P. Vishnu Kamath, C. Shivakumara, *Solid State Sciences* **2005**, *7*, 1180–1187.

[12] C. Taviot-Guého, Y. Feng, A. Faour, F. Leroux, *Dalton Trans.* **2010**, *39*, 5994.
[13] L. Lv, P. Sun, Z. Gu, H. Du, X. Pang, X. Tao, R. Xu, L. Xu, *Journal of Hazardous Materials* **2009**, *161*, 1444–1449.
[14] V. K. Ameena Shirin, R. Sankar, A. P. Johnson, H. V. Gangadharappa, K. Pramod, *Journal of Controlled Release* **2021**, *330*, 398–426.
[15] S.-J. Ryu, H. Jung, J.-M. Oh, J.-K. Lee, J.-H. Choy, *Journal of Physics and Chemistry of Solids* **2010**, *71*, 685–688.
[16] X. Bi, H. Zhang, L. Dou, *Pharmaceutics* **2014**, *6*, 298–332.
[17] K. Zhang, Z. Xu, J. Lu, Z. Tang, H. Zhao, D. Good, M. Wei, *IJMS* **2014**, *15*, 7409–7428.
[18] Y. Zhao, S. He, M. Wei, D. G. Evans, X. Duan, *Chem. Commun.* **2010**, *46*, 3031.
[19] M. Sajid, S. M. Sajid Jillani, N. Baig, K. Alhooshani, *Chemosphere* **2022**, *287*, 132140.
[20] B. M. V. da Gama, R. Selvasembian, D. A. Giannakoudakis, K. S. Triantafyllidis, G. McKay, L. Meili, *Molecules* **2022**, *27*, 4900.
[21] M. Zubair, M. Daud, G. McKay, F. Shehzad, M. A. Al-Harthi, *Applied Clay Science* **2017**, *143*, 279–292.
[22] T. Hibino, *Applied Clay Science* **2015**, *116–117*, 93–101.
[23] Y. Gao, J. Wu, Q. Wang, C. A. Wilkie, D. O'Hare, *J. Mater. Chem. A* **2014**, *2*, 10996.
[24] D. G. Evans, X. Duan, *Chem. Commun.* **2006**, 485–496.
[25] A. Illaik, C. Vuillermoz, S. Commereuc, C. Taviot-Guého, V. Verney, F. Leroux, *Journal of Physics and Chemistry of Solids* **2008**, *69*, 1362–1366.
[26] D. Li, F. Wang, X. Yu, J. Wang, Q. Liu, P. Yang, Y. He, Y. Wang, M. Zhang, *Progress in Organic Coatings* **2011**, *71*, 302–309.
[27] F. Zhang, L. Zhao, H. Chen, S. Xu, D. G. Evans, X. Duan, *Angew. Chem.* **2008**, *120*, 2500–2503.
[28] F. Zhang, M. Sun, S. Xu, L. Zhao, B. Zhang, *Chemical Engineering Journal* **2008**, *141*, 362–367.
[29] S. K. Poznyak, J. Tedim, L. M. Rodrigues, A. N. Salak, M. L. Zheludkevich, L. F. P. Dick, M. G. S. Ferreira, *ACS Appl. Mater. Interfaces* **2009**, *1*, 2353–2362.
[30] H. Ai, X. Huang, Z. Zhu, J. Liu, Q. Chi, Y. Li, Z. Li, X. Ji, *Biosensors and Bioelectronics* **2008**, *24*, 1048–1052.
[31] H. Fan, Y. Li, D. Wu, H. Ma, K. Mao, D. Fan, B. Du, H. Li, Q. Wei, *Analytica Chimica Acta* **2012**, *711*, 24–28.
[32] H. Sohrabi, O. Arbabzadeh, M. Falaki, M. R. Majidi, N. Han, Y. Yoon, A. Khataee, *Food and Chemical Toxicology* **2022**, *164*, 113010.
[33] Y. Wang, Z. Wang, Y. Rui, M. Li, *Biosensors and Bioelectronics* **2015**, *64*, 57–62.
[34] B. Ballarin, M. Morigi, E. Scavetta, R. Seeber, D. Tonelli, *Journal of Electroanalytical Chemistry* **2000**, *492*, 7–14.
[35] C. Mousty, *Applied Clay Science* **2004**, *27*, 159–177.
[36] D. Tang, Y. Han, W. Ji, S. Qiao, X. Zhou, R. Liu, X. Han, H. Huang, Y. Liu, Z. Kang, *Dalton Trans.* **2014**, *43*, 15119–15125.
[37] X. Long, J. Li, S. Xiao, K. Yan, Z. Wang, H. Chen, S. Yang, *Angew. Chem.* **2014**, 5.
[38] Z. Lei, *Journal of Energy Chemistry* **2017**, *26*, 1094–1106.
[39] D. Tang, J. Liu, X. Wu, R. Liu, X. Han, Y. Han, H. Huang, Y. Liu, Z. Kang, *ACS Appl. Mater. Interfaces* **2014**, *6*, 7918–7925.
[40] C. Tang, H.-S. Wang, H.-F. Wang, Q. Zhang, G.-L. Tian, J.-Q. Nie, F. Wei, *Adv. Mater.* **2015**, *27*, 4524–4524.
[41] X. Chen, C. Fu, Y. Wang, W. Yang, D. G. Evans, *Biosensors and Bioelectronics* **2008**, *24*, 356–361.
[42] X. Zou, A. Goswami, T. Asefa, *J. Am. Chem. Soc.* **2013**, *135*, 17242−17245.

[43] B. Ballarin, R. Seeber, D. Tonelli, A. Vaccari, *Journal of Electroanalytical Chemistry* **1999**, *463*, 123–127.
[44] E. Sca, *Electrochimica Acta* **2002**, *47*, 2451–2461.
[45] Y. Li, *Journal of Materials Chemistry A* **2014**, *2*, 13250–13258.
[46] F. Song, *NATURE COMMUNICATIONS* **2014**, *5*, 4477.
[47] H. Wang, X. Xiang, F. Li, *J. Mater. Chem.* **2010**, *20*, 3944.
[48] Z. Li, *Chemical Science* **2015**, 8.
[49] X. Lei, F. Zhang, L. Yang, X. Guo, Y. Tian, S. Fu, F. Li, D. G. Evans, X. Duan, *AIChE J.* **2007**, *53*, 932–940.
[50] K. Ebitani, K. Motokura, K. Mori, T. Mizugaki, K. Kaneda, *J. Org. Chem.* **2006**, *71*, 5440–5447.
[51] H. Chaudhuri, Y.-S. Yun, *Journal of Power Sources* **2023**, *564*, 232870.
[52] M. Shao, R. Zhang, Z. Li, M. Wei, D. G. Evans, X. Duan, *Chem. Commun.* **2015**, *51*, 15880–15893.
[53] E. Shangguan, H. Zhang, C. Wu, X. Cai, Z. Wang, M. Wang, L. Li, G. Wang, Q. Li, J. Li, *Electrochimica Acta* **2020**, *330*, 135198.
[54] A. B. Béléké, E. Higuchi, H. Inoue, M. Mizuhata, *Journal of Power Sources* **2014**, *247*, 572–578.
[55] Z. Zhang, Z. Yang, J. Huang, Z. Feng, X. Xie, *Electrochimica Acta* **2015**, *155*, 61–68.
[56] Y. Liu, Z. Yang, *RSC Adv.* **2016**, *6*, 68584–68591.
[57] J. Liu, Y. Li, X. Huang, G. Li, Z. Li, *Adv. Funct. Mater.* **2008**, *18*, 1448–1458.
[58] B. Yang, Z. Yang, R. Wang, T. Wang, *Electrochimica Acta* **2013**, *111*, 581–587.
[59] M. A. González, R. Trócoli, I. Pavlovic, C. Barriga, F. La Mantia, *Electrochemistry Communications* **2016**, *68*, 1–4.
[60] A. Sumboja, J. Chen, Y. Zong, P. S. Lee, Z. Liu, *Nanoscale* **2017**, *9*, 774–780.
[61] G. A. Caravaggio, C. Detellier, Z. Wronski, *J. Mater. Chem.* **2001**, *11*, 912–921.
[62] X. Long, Z. Wang, S. Xiao, Y. An, S. Yang, *Materials Today* **2016**, *19*, 213–226.
[63] J. He, W. Zhou, D. Zhu, J. Li, Z. Liu, Y. Chen, *ACS Sustainable Chem. Eng.* **2020**, *8*, 14877–14885.
[64] C. Jing, B. Dong, Y. Zhang, *Energy & Environ Materials* **2020**, *3*, 346–379.
[65] L. Zhang, X. Zhang, L. Shen, B. Gao, L. Hao, X. Lu, F. Zhang, B. Ding, C. Yuan, *Journal of Power Sources* **2012**, *199*, 395–401.
[66] X. Zhao, H. Li, M. Zhang, W. Pan, Z. Luo, X. Sun, *ACS Appl. Mater. Interfaces* **2022**, *14*, 34781–34792.
[67] Y. Wang, H. Yang, H. Lv, Z. Zhou, Y. Zhao, H. Wei, Z. Chen, *Journal of Colloid and Interface Science* **2022**, *610*, 35–48.
[68] D. Zhang, X. Guo, X. Tong, Y. Chen, M. Duan, J. Shi, C. Jiang, L. Hu, Q. Kong, J. Zhang, *Journal of Alloys and Compounds* **2020**, *837*, 155529.
[69] R. A. Senthil, A. Min, J. Theerthagiri, G.-A. Kim, H. C. Choi, M. Y. Choi, *Journal of Energy Storage* **2023**, *72*, 108305.
[70] Y. Yao, H. Li, Y. Yu, C. Du, L. Wan, H. Ye, J. Chen, Y. Zhang, M. Xie, *Journal of Energy Storage* **2023**, *59*, 106422.
[71] C.-S. Ni, S.-F. Liu, J.-F. Lee, C.-W. Pao, J.-L. Chen, H.-Y. Chen, J.-H. Huang, *Electrochimica Acta* **2021**, *384*, 138415.
[72] A. D. Deshmukh, A. R. Urade, A. P. Nanwani, K. A. Deshmukh, D. R. Peshwe, P. Sivaraman, S. J. Dhoble, B. K. Gupta, *ACS Omega* **2018**, *3*, 7204–7213.
[73] H. Liang, J. Lin, H. Jia, S. Chen, J. Qi, J. Cao, T. Lin, W. Fei, J. Feng, *Journal of Power Sources* **2018**, *378*, 248–254.
[74] J.-J. Zhou, Q. Li, C. Chen, Y.-L. Li, K. Tao, L. Han, *Chemical Engineering Journal* **2018**, *350*, 551–558.

[75] C. Mousty, S. Therias, C. Forano, J.-P. Besse, *Journal of Electroanalytical Chemistry* **1994**, *374*, 63–69.
[76] J. Sarmet, C. Taviot-Gueho, R. Thirouard, F. Leroux, C. Douard, I. Gaalich, T. Brousse, G. Toussaint, P. Stevens, *Crystal Growth & Design* **2023**, *23*, 2634–2643.
[77] P. Gerlach, C. Douard, I. Gaalich, L. Athouël, J. Sarmet, F. Leroux, C. Tavoit-Gueho, P. Stevens, G. Toussaint, T. Brousse, *J. Electrochem. Soc.* **2023**, *170*, 070505.
[78] J. Sarmet, F. Leroux, C. Taviot-Gueho, P. Gerlach, C. Douard, T. Brousse, G. Toussaint, P. Stevens, *Molecules* **2023**, *28*, 1006.
[79] P. Gerlach, C. Douard, J. Sarmet, F. Leroux, C. Tavoit- Gueho, P. Stevens, G. Toussaint, T. Brousse, *Batteries & Supercaps* **2025**, e202400256.
[80] J. Sarmet, F. Leroux, C. Taviot Gueho, P. Gerlach, C. Douard, T. Brousse, G. Toussaint, P. Stevens, *Journal of Solid State Chemistry* **2024**, *332*, 124592.
[81] C. Li, C. Zhang, J. Xie, K. Wang, J. Li, Q. Zhang, *Chemical Engineering Journal* **2021**, *404*, 126463.
[82] C. Li, H. Yang, J. Xie, K. Wang, J. Li, Q. Zhang, *ACS Appl. Mater. Interfaces* **2020**, *12*, 32719–32725.
[83] J. Xiang, K. Sato, H. Tokue, K. Oyaizu, C. Ho, H. Nishide, W. Wong, M. Wei, *Eur. J. Inorg. Chem.* **2016**, *2016*, 1030–1035.
[84] Y. Ding, Y. Zhao, G. Yu, *Nano Lett.* **2015**, *15*, 4108–4113.
[85] P. S. Borchers, M. Strumpf, C. Friebe, I. Nischang, M. D. Hager, J. Elbert, U. S. Schubert, *Adv. Energy Mater.* **2020**, *10*, 2001825.
[86] Q. Chen, Y. Li, Y. Liu, P. Sun, Z. Yang, T. Xu, *ChemSusChem* **2021**, *14*, 1295–1301.
[87] Y. Zhen, C. Zhang, J. Yuan, Y. Zhao, Y. Li, *Journal of Power Sources* **2020**, *480*, 229132.
[88] Z. Zhao, B. Zhang, B. R. Schrage, C. J. Ziegler, A. Boika, *ACS Appl. Energy Mater.* **2020**, *3*, 10270–10277.
[89] J. Yue, J. Zhang, Y. Tong, M. Chen, L. Liu, L. Jiang, T. Lv, Y. Hu, H. Li, X. Huang, L. Gu, G. Feng, K. Xu, L. Suo, L. Chen, *Nature Chemistry* **2021**, *13*, 1061–1069.
[90] J. Han, A. Mariani, S. Passerini, A. Varzi, *Energy Environ. Sci.* **2023**, *16*, 1480–1501.
[91] M. Amiri, D. Bélanger, *ChemSusChem* **2021**, *14*, 2487–2500.
[92] L. Suo, O. Borodin, T. Gao, M. Olguin, J. Ho, X. Fan, C. Luo, C. Wang, K. Xu, *Science* **2015**, *350*, 938–943.
[93] P. Lannelongue, R. Bouchal, E. Mourad, C. Bodin, M. Olarte, S. le Vot, F. Favier, O. Fontaine, *Journal of The Electrochemical Society* **2018**, *165*, A657.